Novel balanced diplexer with band design flexibility

A. Corona-Chavez[a,b,*], Tejinder Kaur Kataria[b] and J.L. Olvera-Cervantes[a]
[a]*Departamento de Electrónica, Instituto Nacional de Astrofísica, Óptica y Electrónica, Luis Enrique Erro 1, Puebla, 72000, Mexico.*
[b]*Depto. de Electrónica, División de Ingenierías, Universidad de Guanajuato*
[*]*e-mail: alonsocorona@ieee.org*

Received 21 August 2015; accepted 14 March 2016

In this paper a novel differential mode diplexer is presented. This circuit allows complete design independence between both bands. It will be shown that the diplexer can be designed to provide single-ended or differential outputs while having a differential input. All circuits are suitable for 2D fabrication.

Keywords: Balanced filters; diplexers; common mode; differential mode.

PACS: 84.40.Dc; 84.40.Lj

1. Introduction

In modern wireless communication systems, where multi-band capabilities are required, the diplexer is an essential component of the Radio Frequency front-end. In addition, for higher noise immunity, balanced circuits offer common mode (CM) noise suppression [1].

Several active components such as low noise amplifiers (LNA), mixers, and voltage control oscillators have been developed as balanced circuits in order to reduce common-mode noise [2,3]. However, in most of the high frequency literature, single-ended filters and diplexers have dominated the field [4,5]. In order to interconnect such single ended passive devices to balanced LNAs, baluns are necessary as shown in Fig. 1a. Neverheless, the addition of baluns results in larger circuits. For this reason, in recent years, balanced filters and diplexers have been proposed in the literature eliminating the need for baluns and therefore, obtaining system miniaturization [6,7]. Figure 1b and 1c, show a scheme where all the front end components work in balanced mode.

In Refs. 7 to 9, diplexers suitable for an unbalanced antenna and balanced output are shown. However, it is not possible to have all balanced ports. In Ref. 10 another planar configuration is presented where either differential antenna input or differential filter output is possible; however complete differential ports are not supported. In Ref. 11 a diplexer with differential input for all ports is presented but it is not suitable for narrow-band applications. Moreover, a narrow-band full differential diplexer is proposed in Ref. 12; however as it requires via holes, it is not suitable for 2D fabrication. In Ref. 13 another all-port differential diplexer is presented; nevertheless, its contra-directional outputs make it unsuitable for complete planar integration to other components.

In this paper we present a novel balanced diplexer topology that allows to have a balanced antenna input [14,15], while having either one or both balanced outputs at the filters. In addition, this topology allows 2D fabrication and planar integration to other components. To the auhors' knowledge, this is the first paper decribing a topology supporitng a balanced antenna and allowing any of the filter outputs to be balanced without using baluns. As summarized on Table I, the topology presented in this paper is the only one supporting a balanced antenna input while having the choice of selecting the type of filter output as balanced or unbalanced.

For demonstration, two circuits are presented in this paper, the first one has a differential antenna input, and both filter outputs have single ended connections. The second diplexer has a differential antenna input, one filter with differential output and the other one with single ended terminals.

TABLE I.

Reference	Balanced antenna input	Balanced filter output	Single ended filter output	All balanced outputs	Narrow band	2D integration
7-9	No	Yes	No	No	Yes	Yes
10	No	Yes	No	No	Yes	Yes
11	Yes	Yes	No	Yes	No	Yes
12	Yes	Yes	No	Yes	Yes	No
13	Yes	Yes	No	Yes	Yes	No
This work	Yes	Yes	Yes	Yes	Yes	Yes

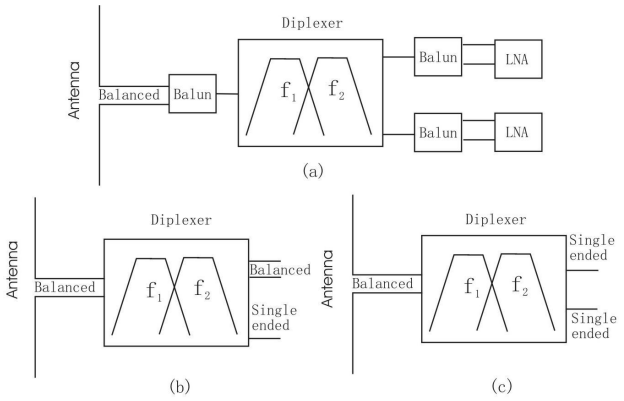

FIGURE 1. Different Front end configurations for balanced circuits.

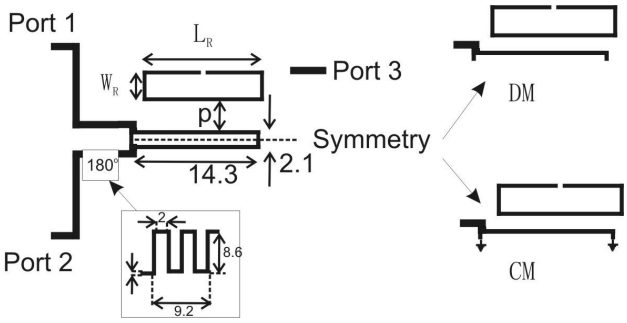

FIGURE 2. Novel feed showing its differential and common mode behavior. (All dimensions are in mm).

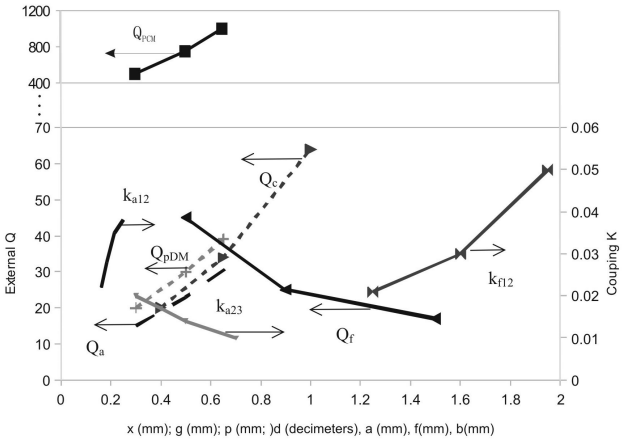

FIGURE 3. External couplings (Q) and resonator couplings (k) for different configurations of hairpin resonator.

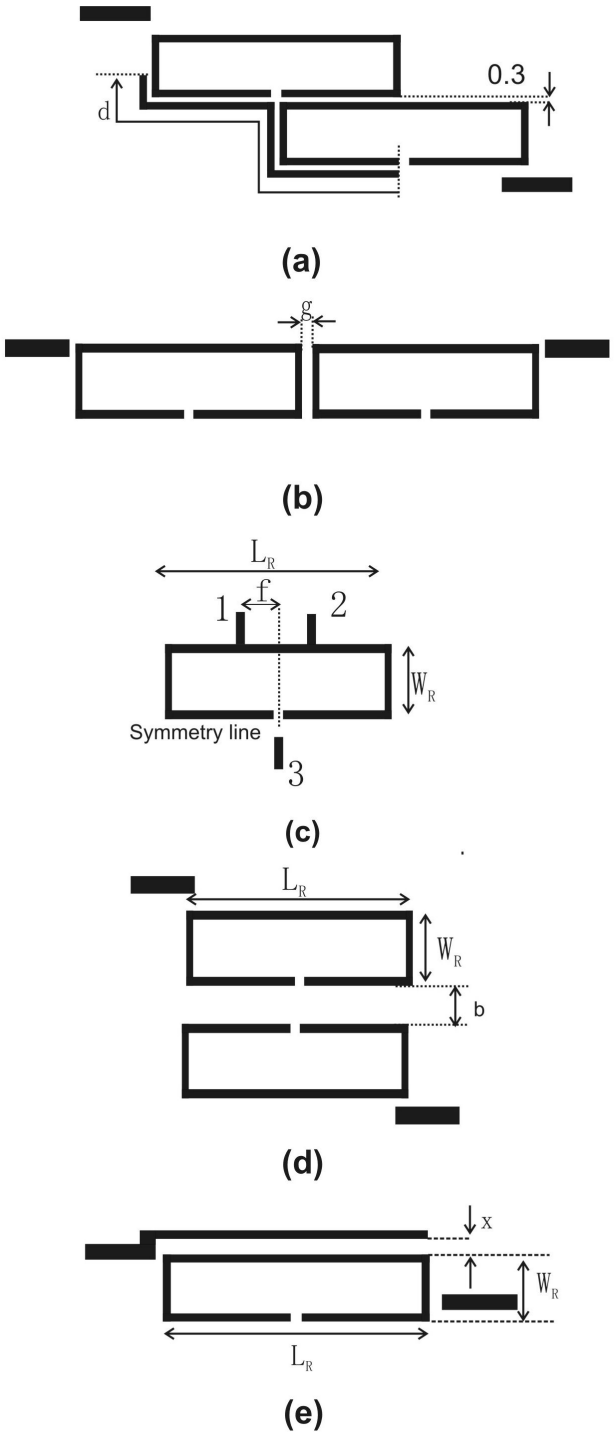

FIGURE 4. (a) Differential coupling of hairpin resonator using novel feed; (b) and (c) mutual coupling configuration; (d) differential external coupling; (e) mutual coupling; and (f) single ended external coupling. All dimensions are in millimeters.

2. Novel feed

To feed the circuit we use a 0° and a 180° delay lines that change the polarity of the input signal as shown in Fig. 2. This structure is then connected to a coupling ring. Depending on the input condition, this ring will have an open or short circuit at the line of symmetry. For a CM input signal, a short circuit is forced along the symmetry line, therefore the coupled signal to the resonator is highly attenuated. On the contrary, for a differential mode (DM) signal, an open circuit is forced at the symmetry line therefore coupling the signal to the resonator

To investigate the coupling characteristics, a 180° meander microstrip line was designed on a substrate with

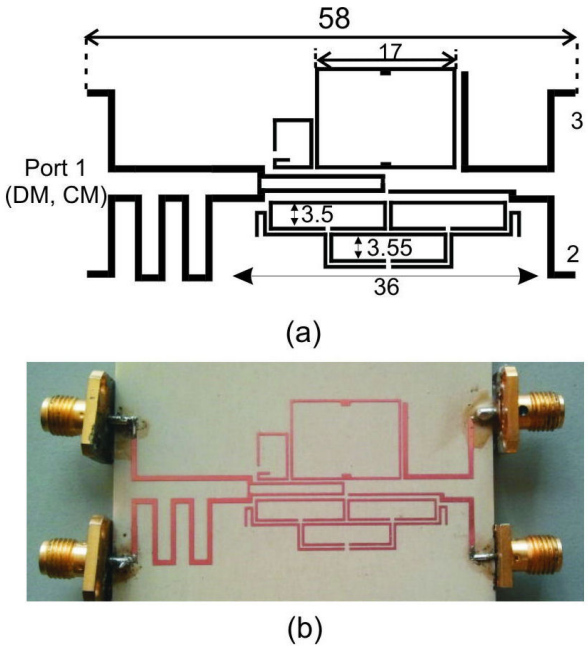

FIGURE 5. (a) Layout and (b) picture of diplexer with 3 pole hairpin filter and 2 pole ring filter. All dimensions are in mm.

$\varepsilon r = 10.2$ and thickness h=1.27 mm at 2 GHz and a hairpin resonator was coupled to it. Another weakly coupled line was added as shown In Fig. 1. Here, $L_R = 14$ mm and $W_R = 3.5$ mm. The structure was simulated in Ref. 16 by changing the distance p from 0.3 to 0.65 mm. Then, the S parameters were imported in Ref. 17 where an ideal rat-race coupler is connected to ports 1 and 2 to operate the circuit in CM or DM mode. By choosing the right input port of the coupler, its outputs will give 180° (for the differential mode operation) and 0° for the common mode operation. By following the procedure shown in Ref. 18, the DM and CM external Q values are obtained (Q_{pDM} and Q_{pCM}). The results are shown in Fig. 3. The DM Q factor (Q_{pDM}) changes from 20 to 40. For the same case, the CM changes from 500 to 1000, therefore CM is highly attenuated.

3. Diplexer with differential input and single ended outputs

The first diplexer to be presented has a differential input and two single ended outputs. Fort the first band, a filter at a center frequency $f_o = 1.85$ GHz, FBW = 3.7% with a 3 pole asynchronously tuned response is chosen. This filter has a transmission zero at 1.95 GHz. The coupling matrix (1) is obtained by optimization [18]

From (1), our required external coupling becomes $Q_{p-DM} = 27$ therefore we use $p = 0.5$ mm (from Fig. 3). In this case Q_{p-CM} is 750.

To calculate the gap between the first and second resonators, the structure in Fig. 4a is simulated in Ref. 16 at different lengths d. The mutual coupling coefficients (k_{a12}) are plotted in Fig. 3. In our case, $k_{a12} = 0.036$, therefore $d = 25$ mm.

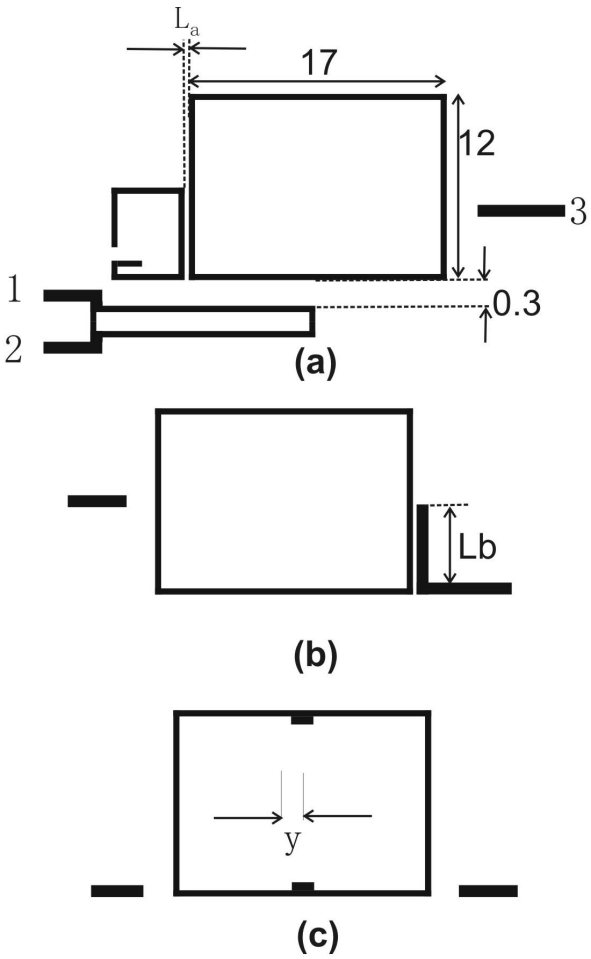

FIGURE 6. (a) External differential coupling of ring-resonator; (b) single-ended external coupling; and (c) mutual coupling. All dimensions are in mm.

To calculate the cross-coupling k_{a23}, the structure in Fig. 4b is simulated in Ref. 16 for different gaps g and the results are depicted in Fig. 3. For our requirement, $k_{a23} = 0.014$ hence $g = 0.5$ mm.

$$k_a = \begin{pmatrix} 0.09 & 0.98 & 0.36 \\ 0.98 & -0.35 & 0.98 \\ 0.36 & 0.98 & 0.09 \end{pmatrix} \quad (1)$$

For the single-ended output external coupling (Fig. 4e), the required dimension for a $Q_a = 27$, is $x = 0.56$ mm (Fig. 3). To adjust the position of the transmission zero, the second resonator's width was slightly changed as seen in Fig. 5.

For the second band we will use a 2 pole Chebyshev filter using ring resonators centered at $f_o = 2.06$ GHz and FBW = 1.97%. A transmission zero is added at 2 GHz [19].

Firstly, we obtain the low pass prototype g values from [20] for a 0.1 dB ripple, which are: $g_o = 1$, $g_1 = 0.843$, $g_2 = 0.622$ and $g_3 = 1.355$. Then, we calculate the mutual coupling between the ith and jth resonators (k_{ij}) and external coupling (Q) using (2) and (3) respectively

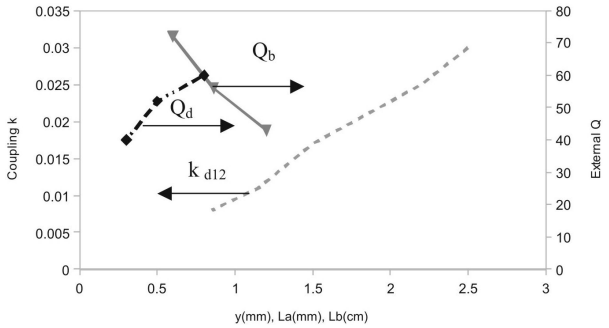

FIGURE 7. External couplings (Q) and resonator couplings (k) for different configurations of ring resonator.

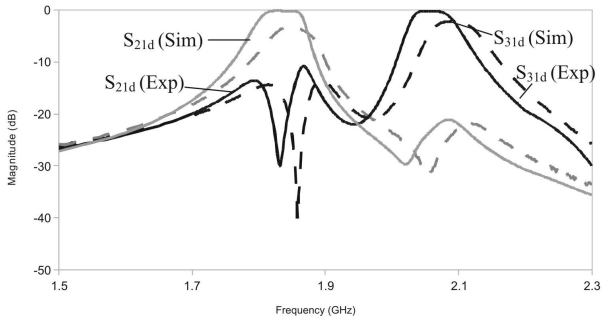

FIGURE 8. Experimental and simulated differential insertion losses of diplexer with differential input and single ended outputs.

$$Q = \frac{g_0 g_n}{\text{FBW}} \tag{2}$$

$$k_{ij} = \frac{\text{FBW}}{\sqrt{g_i g_j}} \tag{3}$$

Where g_n is the nth g parameter for an nth order filter, g_i is the g value of the ith resonator and g_j for the jth resonator.

For our requirement, the external DM quality factor is $Q_d = 43$ and the mutual coupling coefficient Is $k_{c12} = 0.027$. To obtain the physical layout we simulate the structure in Fig. 6a in Ref. 16 for different values of La. The results are plotted in Fig. 7. For our requirement $L_a = 0.4$ mm. For this structure, the DM external coupling is 1250, therefore the DM is highly attenuated. Similarly, to calculate the mutual coupling, the structure in Fig. 6b was simulated In Ref. 16 for different notch widths (y) and the results are plotted in Fig. 7. Our final value is $y = 2$ mm. For the output coupling (Fig. 5b), the extracted external Q values plotted versus the length L_b are shown in Fig. 7. For our required $Q_b = 43$ we get $L_b = 12$ mm. The final filter layout is shown in Fig. 5.

The diplexer was fined tuned in Ref. 16 and then fabricated using photo-lithography (Fig. 5b). All the ports were measured with a 2 port Vector Network Analyzer and the unconnected ports were connected to a 50 Ω load. In order to obtain the final Differential and Common Mode responses, the experimental measurements were imported into [17] and an ideal 180° hybrid coupler was used to activate DM or CM respectively. The final experimental and simulated results are shown in Fig. 8.

For the first passband, the experimental center frequency is 1.85 GHz with an insertion loss (S_{21d}) of 3.2 dB. For the second passband the experimental center frequency is 2.09 GHz with an insertion loss (S_{31d}) of 2.5 dB. The experimental and simulated differential return losses (S_{11d}) are better than 15 dB for both bands (Fig. 8). The CM insertion losses for the lower band filter (S_{21c}) are better than 18 dB for the simulation and 20 dB for the experiment. For the second filter (S_{31c}), the simulation insertion losses are greater than 13 dB and the experimental are greater than 16 dB.

It is important to note that the simulation results assume lossless conductors and dielectrics, resulting in much higher experimental losses. In addition, no filter tuning was per-

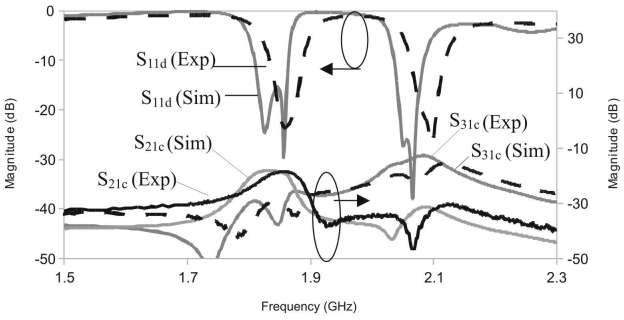

FIGURE 9. Experimental and simulated differential return losses of diplexer with differential input and single ended outputs plus its common mode response.

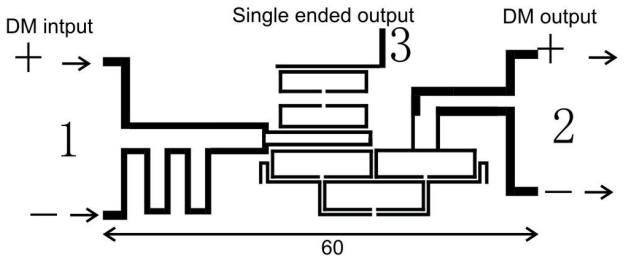

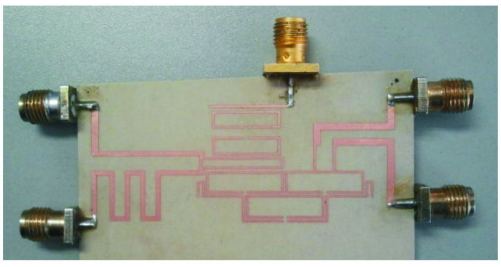

FIGURE 10. (a) Layout of diplexer with differential input and differential/single-ended outputs; (b) Fabricated diplexer. All dimensions are in mm.

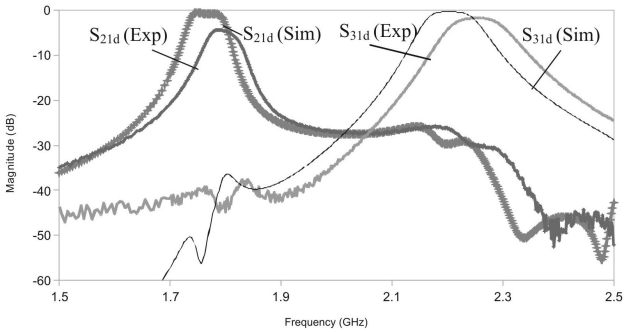

FIGURE 11. Experimental and simulated differential insertion losses of diplexer with differential input and differential/single-ended outputs.

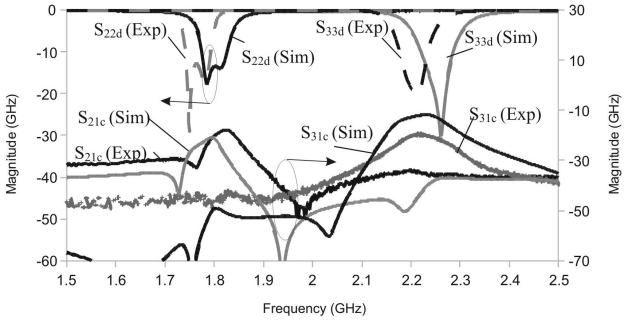

FIGURE 12. Experimental and simulated differential return losses of diplexer with differential input and differential/single-ended outputs; and its common mode response.

formed during the experiment, for that reason, the differences between simulated and experimental results can also be attributed to manufacturing errors during the photolitograhy process, as well as material tolerances such as substrate thickness and permittivity.

4. Diplexer with differential input, one single ended output and a differential output

As previously discussed, this topology is suitable for any type of output according to the chosen resonator. In this section we will describe the circuit having a differential antenna input, one differential output and one single ended output.

The 3 pole filter described in the previous section will be used at a center frequency $f_o = 1.77$ GHz and having a differential output. For this, the output coupling was changed to the one shown in Fig. 4c as previously reported in Ref. 6. In this case, a differential signal will force a short circuit at the symmetry line. In order to extract the $Q_f = 27$ parameter, the distance f was varied and simulated in Ref. 16. Then, from Fig. 3 the value of f is calculated as $f = 1.0$ mm. In this case $L_R = 14$ mm and $W_R = 4$ mm.

For the single ended output a 2-pole Chebyshev filter was designed at $f_o = 2.2$ GHz with a fractional bandwidth FBW = 2.3%. The g values are described in Sec. 3. This leads to an external quality factor, $Q_c = 37$ and a coupling factor $k_{f12} = 0.03$. In order to couple the circuit, the configuration shown in Fig. 4e was simulated at different x values. From Fig. 3, for the required Q_c, x is 0.66 mm.

To obtain the mutual coupling value, the structure in Fig. 4d was simulated for different b values. The required b distance is extracted from Fig. 3 as $b = 1.6$ mm. Finally, for the differential input coupling, the structure of Fig. 2 is used and the gap value (p) is extracted from Fig. 3 as 0.6 mm. In this case $L_R = 12.2$ mm and $W_R = 3.2$.

The final filter layout and the fabricated prototype are shown in Fig. 10. To measure the filter a similar technique as in the previous sections was used. The simulation and experimental results are shown in Fig. 11 and 12.

For the first passband, the experimental center frequency is 1.78 GHz with an insertion loss (S_{21d}) of 4 dB. For the second passband the experimental center frequency is 2.25 GHz with an insertion loss (S_{31d}) of 1.6 dB. The experimental and simulated differential return losses at the filter output ports (S_{22d} and S_{33d}) are better than 14 dB for both bands (Fig. 12).

The CM insertion losses for the lower band filter (S_{21c}) are better than 21 dB for the simulation and 18 dB for the experiment. For the second filter (S_{31c}), the simulation has insertion losses greater than 12 dB and the experiment greater than 19 dB.

As in the previous circuit, perfect conductor and dielectric were assumed in the simulation, for that reason, insertion losses are much higher in the experiment. In addition, no tunning was performed during the experiment. The differences between simulated and experimental results are attributed to manufacturing and material tolerances.

5. Conclusions

In this paper a novel differential mode diplexer topology has been presented. This structure allows complete design independence between both diplexer bands. In addition, this feed can be combined to provide single- ended or differential outputs while having a differential input. Two diplexers were shown, one has a differential input, and single-ended outputs; the other one has differential input, a single ended output and a differential output. All structures presented agreeable results between experiment and simulations

1. E. Bogatin, *Signal Integrity-Simplified ser. Modern Semiconductor Design Series*, Englewood Cliffs, NJ, USA: Prentice Hall, (2004).

2. N. Wadefalk, P.S. Kildal, and H. Zirath, *A low noise integrated 0.3-16 ghz differential amplifier for balanced ultra wideband antennas, In: Proceedings of the IEEE Compound Semicon-*

ductor Integrated Circuit Symposium (CSICS) (2010) pp. 1-4.

3. X.B. Li, M.J. Zhao, Z.H. Wu, and B. Li, *A high-linearity fully-differential mixer, In: Proceedings of the International Conference of Electron Devices and Solid-State Circuits (EDSSC)*, (2011) pp. 1-2.
4. Shang, Xiaobang, Yi Wang, Wenlin Xia, and M.J. Lancaster, *Microwave Theory and Techniques IEEE Transactions on 61*, (2013) 3838-3845.
5. J.R. Loo-Yau, O.I. Gómez-Pichardo, F. Sandoval-Ibarra, M.C. Maya-Sánchez, and J.A. Reynoso-Hernández, *Rev. Mex. Fis.* **57** (2011) 184-187.
6. J.-L. Olvera-Cervantes, and A. Corona-Chavez, *Microwave and Wireless Components Letters, IEEE* **23** (2013) 530-532.
7. C.H. Wu, C.H. Wang, and C.H. Chen, *A novel balanced-to-unbalanced diplexer based on four-port balanced-to-balanced band-pass filter, In: Proceedings of the 38th European Microwave Conference (EuMC)*, Amsterdam, The Netherlands, (October 2008) pp. 28-31.
8. Bao, Zhi-Hua, Ji-Xin Chen, Eng Hock Lim, and Quan Xue, *Electronics Letters* **46** (2010) 766-768.
9. Chen, Chia-Mao, Shoou-Jinn Chang, Cheng-Fu Yang, and Cheng-Yi Chen, *A Simple and Effective Method for Designing Frequency Adjustable Balun Diplexer With High Common-Mode Suppression* (2015).
10. Q. Xue, J. Shi, and J.X. Chen, *IEEE Trans Microwave Theory Tech* **59** (2011) 2848-2855.
11. H. Lobato Morales, S. Sun Jim, A. Corona Chavez, T. Itoh, J.L. Olvera Cervantes, *IEEE MTT-S International*, Montreal, Canada, (2012) pp. 1-3.
12. H. Deng, Y. Zhao, Y. Fu, Y. He, and X. Zhao, *J. Electromagn Waves Appl* **27** (2013) 1047-1058.
13. Arbelaez Nieto, Arcesio *et al*., *Microwave and Optical Technology Letters* **57.3** (2015) 567-570.
14. Kaur, Rupinder, and Munish Rattan, *Wireless Personal Communications* (2014) 1-10.
15. E. Colín-Beltrán, A. Corona-Chávez, T. Itoh, and J. Eduardo Mendoza-Torres, *IEEE Transactions on 61* (2013) 2425-2431.
16. SONNET 7.0b. Sonnet Software Inc., (Pittsburgh, PA, 2001).
17. AWR Microwave Office (2002).
18. Hong, Jia-Shen G. and M.J. Lancaster, *Microstrip filters for RF/microwave applications* **167** (John Wiley & Sons, 2004).
19. Salleh, M.K Mohd *et al*., *Microwave Theory and Techniques, IEEE transactions on 56.1* (2008) 156-162.
20. G.L. Matthaei, L. Young, Jones EMT., *Microwave filters, impedance-matching networks, and coupling structures*. Norwood (MA): (Artech House; 1980).